



HAL
open science

Tunneling anisotropic spin galvanic effect

Geneviève Fleury, Michael Barth, Cosimo Gorini

► **To cite this version:**

Geneviève Fleury, Michael Barth, Cosimo Gorini. Tunneling anisotropic spin galvanic effect. 2023. hal-03939261

HAL Id: hal-03939261

<https://hal.science/hal-03939261>

Preprint submitted on 14 Jan 2023

HAL is a multi-disciplinary open access archive for the deposit and dissemination of scientific research documents, whether they are published or not. The documents may come from teaching and research institutions in France or abroad, or from public or private research centers.

L'archive ouverte pluridisciplinaire **HAL**, est destinée au dépôt et à la diffusion de documents scientifiques de niveau recherche, publiés ou non, émanant des établissements d'enseignement et de recherche français ou étrangers, des laboratoires publics ou privés.

Tunneling anisotropic spin galvanic effect

Geneviève Fleury,¹ Michael Barth,² and Cosimo Gorini^{1,*}

¹*SPEC, CEA, CNRS, Université Paris-Saclay, 91191 Gif-sur-Yvette, France*

²*Institut für Theoretische Physik, Universität Regensburg, 93040 Regensburg, Germany*

(Dated: December 23, 2022)

We show that pure spin injection from a magnetic electrode into an inversion symmetry-broken system composed of a tunnelling barrier and a metallic region generates a transverse charge current. Such a tunnelling spin galvanic conversion is non-local and may be strongly anisotropic even in linear response, contrary to what happens in bulk conversion setups lacking tunnelling elements. This is particularly relevant for spin-charge conversion at oxide interfaces, where both the tunnel barrier and the receiving low-dimensional metallic system host effective spin-orbit fields with complex angular symmetries.

Spin-orbit (SO) coupling in metallic systems offers many possibilities for converting spin signals into charge ones and vice-versa [1, 2]. In particular, charge currents may be generated by pure spin injection via the spin galvanic effect (SGE) [3–7] – the conversion of a non-equilibrium spin accumulation into a charge current – and/or the inverse spin Hall effect (ISHE) [2, 8–11] – the conversion of a pure spin flow into a transverse charge flow. The working principle of the typical spin pumping setup, sketched in Fig. 1, relies on both phenomena: a magnetic electrode is driven by microwaves, and its precessing magnetization injects angular momentum – but on average no charges – into an underlying metallic system, where SO converts it into a measurable electric voltage. Broadly speaking, there are two scenarios: (i) The receiving system is 3D, so that pumping results in a pure spin current flowing away from the magnet. This is the case for popular metal-based setups, where the bulk ISHE dominates spin-charge conversion[10–14]; (ii) The receiver has no thickness through which an injected spin current may flow, *e.g.* it is a 2D electron gas (2DEG) at an interface or on the surface of a 3D topological insulator. In this case the absorbed angular momentum builds up a spin accumulation, which is converted into a voltage by the SGE[15–17]. If the importance of interfacial SO à la Rashba [18, 19] is agreed upon, the situation is in practice not always that clear-cut. This leaves room for debate concerning the dominance of specific conversion channels, as both bulk and interfacial contributions may exist and compete [2, 19–22].

A further layer of complexity is added by the injection process itself, which happens through an inversion-asymmetric magnetic tunnel junction. Due to the interplay of magnetism and interfacial SO from inversion symmetry breaking, junctions of these sort host a plethora of anisotropic magneto-electric effects [20, 23, 24]. Very recently, some tunneling spin Hall and anomalous Hall effects were proposed [25], arising from under-the-barrier transmission which is not only spin-sensitive, but also skewed in momentum space[26]. Skewedness actually appears also if SO is present only on the injecting/receiving metallic sides [27–29], rather than only under the barrier

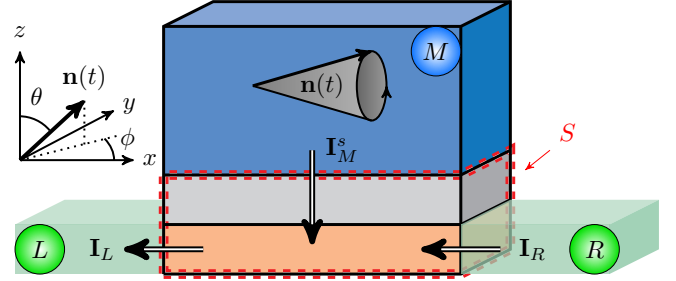


FIG. 1. Spin pumping setup: the top magnetic (M) and two left (L) and right (R) normal electrodes are connected to a scattering region S marked by the red dashed line. S consists of a tunnel barrier (gray) on top of a metallic layer (orange). SO from inversion-symmetry breaking along z may be active in the barrier, in the underlying layer or in both. The M electrode is driven and can inject/absorb spins but no charges. The spin-charge conversion voltage is measured between the L and R electrodes as a function of $\mathbf{n}_0(\theta, \phi)$, *i.e.* the rest direction of the magnetization in absence of driving.

[25]. As emphasised in Ref. [29], skewed injection is crucial in a novel spin-charge conversion platform rapidly on the rise: that of high-quality 2DEGs at oxide interfaces [30], whose fundamental and technological potential is beyond question [31–33]. Such systems can be easily manipulated via gates and are intrinsically inversion-asymmetric, with more or less complex forms of Rashba SO on the 2DEG side[32, 34, 35]. Closely related systems also host various exotic transport phenomena [33, 36, 37].

A recent experiment showed that spin-charge conversion in a LAO|STO 2DEG is indeed strongly anisotropic, carrying imprints of the spin texture of the effective Rashba field [38][39]. This contrasts with the known fact that the Onsager reciprocal phenomenon – the generation of a non-equilibrium spin accumulation by driving a current – is isotropic in the very same kind of systems, independently of the Rashba texture [40]. Furthermore, at an oxide interface Rashba SO is present not only on the 2DEG side, but also in the barrier separating it from the spin pumper[38], and both may contribute to spin-charge (charge-spin) conversion.

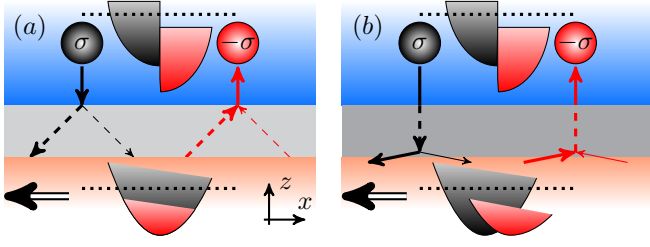


FIG. 2. Inversion symmetry-broken magnetic tunnel junction under a pure spin bias (same color code from Fig. 1). The black dotted lines mark the electrochemical potential $\mu_{L,\sigma} = \mu_{L,-\sigma} = \mu_{R,\sigma} = \mu_{R,-\sigma} = \mu + \delta\mu$ of the side electrodes, which floats to ensure overall charge neutrality. Mott skew scattering results from spin-momentum correlations induced by SO when electrons imping on impurities[8]. Similar correlations appear if electrons cross any scattering region with SO, *e.g.* by tunneling through a SO-coupled barrier [24, 25] or by entering from/landing into a region with SO [27–29], leading to various spin-charge conversion channels. (a): SO is present only in the barrier, where a tunnelling ISHE takes place. The resulting skewed populations of both spin-degenerate bands yield a transverse charge current. Note that the non-equilibrium spin accumulation induced by pumping is not converted into a current, *i.e.* there is no SGE on the receiving side. (b): SO is present only on the receiving side. Skewed injection takes place at the exit of the barrier, causing an asymmetric population of the (Rashba) spin-split bands. Such asymmetric band filling is qualitatively analogous to the one induced by spin relaxation in the standard SGE [3–5, 41], but is here uniquely due to skew tunneling. The usual spin relaxation channel is however active as well, since SO is present on the receiving side, and will also affect the overall SGE of the junction. In a general inversion-asymmetric junction both (a) and (b) mechanisms are present, yielding an overall “tunneling anisotropic SGE”.

Our goal is two-fold. First, we build a theory framework describing spin-charge conversion in inversion symmetry-broken multi-terminal setups, in which a driven magnetic electrode acts as a pure spin injector. Onsager reciprocity is fulfilled by construction. The theory also treats tunnel and receiving elements on the same footing, thus including SO effects and magnetic correlations in either or both, and can be straightforwardly extended to consider *e.g.* superconducting contacts. Second, we provide a microscopic description of recent experiments, by applying the general theory to a model system of an oxide interface junction. In so doing we identify a spin-charge conversion channel which mixes skew-tunneling and standard SGE physics, and which we refer to in the following as “tunneling anisotropic SGE” – see Eq. (7). The proposed effect works on general principles, sketched in Fig. 2 and discussed in its caption. It should thus appear in any magnetic tunnel junction with broken inversion symmetry under a spin bias.

Steady state transport theory – Without loss of generality we first focus on the essentials and consider the three-terminal system from Fig. 1. Since we are interested

in the DC output of the setup, we reformulate the time-dependent spin pumping problem from the start as an effective steady-state problem. This substantial simplification allows us to proceed via time-independent scattering theory – much simpler and numerically cheaper than any time-dependent approach. The magnet hosts free electrons whose spin σ couples to the magnetization via standard *s-d* exchange $H_{xc} = -(\Delta_{xc}/2)\mathbf{n}(\theta, \phi) \cdot \boldsymbol{\sigma}$, $|\mathbf{n}| = 1$. The magnetization angles θ, ϕ are defined as usual, see Fig. 1. Under driving the magnetization precesses, $\mathbf{n} \rightarrow \mathbf{n}(t)$, producing in the magnet a non-equilibrium spin polarisation (density) $\delta\mathbf{s}(t) = \hbar N_0/2 [\mathbf{n} \times \dot{\mathbf{n}} - (\hbar/\Delta_{xc}\tau_s)\dot{\mathbf{n}}]$, with N_0 the density of states per spin and unit volume at the Fermi energy, and τ_s the spin relaxation time. Such spin polarization has a steady-state component $\overline{\delta\mathbf{s}} = \hbar N_0/2 [\mathbf{n} \times \dot{\mathbf{n}}]$. The latter can be used to define an effective spin electrochemical potential proportional to the driving frequency ω [41, 42]

$$\overline{\mathbf{n} \times \dot{\mathbf{n}}} \equiv \delta\boldsymbol{\mu}_s. \quad (1)$$

The spin pumper thus acts as a magnetic electrode under a pure steady-state spin bias. It is easy to see that $\delta\boldsymbol{\mu}_s$ is parallel to the (arbitrary) rest direction \mathbf{n}_0 of the magnetization, since misaligned spins relax too fast to allow any buildup [41, 42]. We thus have $\delta\boldsymbol{\mu}_s = \delta\mu_M^\uparrow - \delta\mu_M^\downarrow$, where $\delta\mu_M^\sigma$, $\sigma = \uparrow, \downarrow$ is the deviation from equilibrium of the electrochemical potential for \mathbf{n}_0 -polarized majority/minority electrons. The σ -polarized currents flowing into/out of the 3-terminal setup of Fig. 1 are written in Landauer-Büttiker form following Ref. [43]

$$I_\alpha^\sigma = \frac{e}{h} \sum_{\beta, \sigma' = \uparrow\downarrow} \int d\epsilon [f(\epsilon, \mu_\alpha^\sigma) - f(\epsilon, \mu_\beta^{\sigma'})] T_{\alpha\beta}^{\sigma\sigma'}(\epsilon). \quad (2)$$

Here $T_{\alpha\beta}^{\sigma\sigma'}$ is the transmission probability from lead β with spin σ' to lead α with spin σ , and $f(\epsilon, \mu) = [1 + e^{(\epsilon - \mu)/(k_B T)}]$ is the Fermi function, T being the (uniform) temperature and k_B the Boltzmann constant. In our configuration the left and right ($\alpha = L, R$) normal electrodes are at the same electrochemical potential $\mu_L^\sigma = \mu_L^{\bar{\sigma}} = \mu_R^\sigma = \mu_R^{\bar{\sigma}} \equiv \mu + \delta\mu$, with $\bar{\sigma} \equiv -\sigma$, while in the magnetic ($\alpha = M$) terminal $\mu_M^\sigma = \mu + \delta\mu_M^\sigma$. Linear response (small $\delta\mu, \delta\mu_M^\sigma$) yields

$$I_\alpha^\sigma = \sum_{\sigma'} \left(\frac{\delta\mu_M^{\sigma'} - \delta\mu}{e} \right) G_{\alpha M}^{\sigma\sigma'}, \quad \alpha = L, R \quad (3)$$

in the normal electrodes, and in the magnetic one

$$I_M^\sigma = \left(\frac{\delta\mu - \delta\mu_M^\sigma}{e} \right) \sum_{\sigma'} [G_{ML}^{\sigma\sigma'} + G_{MR}^{\sigma\sigma'}] + \left(\frac{\delta\mu_M^{\bar{\sigma}} - \delta\mu_M^\sigma}{e} \right) G_{M\bar{M}}^{\sigma\bar{\sigma}} \quad (4)$$

With f_0 the equilibrium distribution, the conductances are

$$G_{\alpha\beta}^{\sigma\sigma'} = \frac{e^2}{h} \int d\epsilon \left(-\frac{\partial f_0}{\partial \epsilon} \right) T_{\alpha\beta}^{\sigma\sigma'}. \quad (5)$$

Charge conservation dictates that the currents $I_\alpha = \sum_\sigma I_\alpha^\sigma$ add up to zero, $I_M + I_L + I_R = 0$. Furthermore, the pumping electrode remains charge neutral on average, *i.e.* $I_M = 0$ [44]. Lengthy but straightforward calculations allow to write the spin current in lead M ($I_M^s \equiv (\hbar/2e) [I_M^\uparrow - I_M^\downarrow]$) and the charge currents in the normal leads (I_L, I_R) in response to the spin bias $\delta\mu_s$. The spin-charge conversion current I_{sc} generated by the tunnelling anisotropic SGE is a transverse current. We define it as the difference between L and R currents, $I_{sc} = I_L - I_R$

$$I_{sc} = I_L - I_R = \mathcal{G}_{sc} \delta\mu_s / e. \quad (6)$$

The corresponding conductance \mathcal{G}_{sc} reads

$$\mathcal{G}_{sc} = \frac{\mathbb{G}_{LM} (\mathbb{G}_{RM}^\uparrow - \mathbb{G}_{RM}^\downarrow) - \mathbb{G}_{RM} (\mathbb{G}_{LM}^\uparrow - \mathbb{G}_{LM}^\downarrow)}{\mathbb{G}_M}, \quad (7)$$

having defined $\mathbb{G}_{\alpha M}^\sigma = \sum_{\sigma'} G_{\alpha M}^{\sigma'\sigma}$, $\mathbb{G}_{\alpha M} = \sum_\sigma \mathbb{G}_{\alpha M}^\sigma$, $\mathbb{G}_M = \sum_\alpha \mathbb{G}_{\alpha M}$, with $\alpha = R, L$. In the Onsager reciprocal scenario an electric bias drives a current $R \rightarrow L$, $\mu_L - \mu_R = -\delta\mu_{LR}$ [45], which generates a pure spin current I_M^s into the M electrode. The latter is $I_M^s = (\hbar/2e)I_{cs}$, with I_{cs} the charge-spin (*cs*) conversion current

$$I_{cs} = I_M^\uparrow - I_M^\downarrow = \mathcal{G}_{cs} \delta\mu_{LR} / e. \quad (8)$$

The conductance is

$$\mathcal{G}_{cs} = -\frac{\mathbb{G}_{ML} (\mathbb{G}_{MR}^\uparrow - \mathbb{G}_{MR}^\downarrow) - \mathbb{G}_{MR} (\mathbb{G}_{ML}^\uparrow - \mathbb{G}_{ML}^\downarrow)}{\mathbb{G}_M}, \quad (9)$$

with $\mathbb{G}_{M\alpha}^\sigma = \sum_{\sigma'} G_{M\alpha}^{\sigma'\sigma}$, $\alpha = L, R$. From microreversibility in the presence of exchange interaction one has $G_{\alpha\beta}^{\sigma\sigma'}(\Delta_{xc}) = G_{\beta\alpha}^{\sigma'\sigma}(-\Delta_{xc})$ [46, 47] which leads to the Onsager-Casimir relation for the tunneling SGE

$$\mathcal{G}_{sc}(\Delta_{xc}) = \mathcal{G}_{cs}(-\Delta_{xc}). \quad (10)$$

Eqs. (7), (9) and (10) are central results of our work. They are fully general, *i.e.* independent of any detail of the multi-terminal structure, and their extension to an arbitrary number of electrodes is straightforward. Indeed, we verify Eq. (10) explicitly for our LAO|STO model in a 5-terminal configuration below.

Anisotropies – To explain anisotropic effects in two-terminal magnetic tunnel junctions with SO, Refs. [24 and 25] give arguments which can be generalized to our multi-terminal setup, Fig. 1. To be definite consider the spin-resolved transmission $\mathbb{G}_{\alpha M}^\sigma = \sum_{\sigma'} G_{\alpha M}^{\sigma'\sigma}$, written as

$$\mathbb{G}_{\alpha M}^\sigma = \frac{e^2}{h} \int d\epsilon \left(-\frac{\partial f_0}{\partial \epsilon} \right) \sum_{\mathbf{k}} W_\alpha^\sigma(\epsilon, \mathbf{k}). \quad (11)$$

Here \mathbf{k} labels the propagating modes in lead M , *i.e.* \mathbf{k} is momentum in the x-y junction plane. To establish direct contact with Refs. [24 and 25] we introduced the spin- and momentum-resolved transmission probability $W_\alpha^\sigma(\epsilon, \mathbf{k}) = \sum_{\sigma'} \sum_{\mathbf{q}_\alpha} [t^\dagger t]_{\mathbf{k}\mathbf{q}_\alpha}^{\sigma\sigma'}$, with \mathbf{q}_α the mode label (transverse momentum) in lead α , and t the transmission amplitudes entering the scattering matrix [43, 47]. Without SO the transmission $W_\alpha^\sigma(\epsilon, \mathbf{k})$ is even in \mathbf{k} , $W_\alpha^\sigma(\mathbf{k}) = W_\alpha^\sigma(-\mathbf{k})$. With SO in the scattering region S – either in the barrier, in the 2DEG, or in both – there appears a (Rashba-like) SO field $\mathbf{b}(\mathbf{k})$ such that $\mathbf{b}(\mathbf{k}) = -\mathbf{b}(-\mathbf{k})$, spoiling the $\mathbf{k} \rightarrow -\mathbf{k}$ symmetry of $W_\alpha^\sigma(\epsilon, \mathbf{k})$: transmission is now in general skewed. Indeed, $W_\alpha^\sigma(\epsilon, \mathbf{k})$ is a function of the angle between \mathbf{n} and $\mathbf{b}(\mathbf{k})$, as the magnetization and the SO field define the two physically preferred directions of the problem. Simple manipulations show that such properties are transferred to the conductance \mathcal{G}_{sc} , yielding the formal expansion

$$\mathcal{G}_{sc} = \sum_{\mathbf{k}} \sum_n \mathcal{G}_{sc}^{(n)} [\mathbf{n} \cdot \mathbf{b}(\mathbf{k})]^n. \quad (12)$$

Odd terms vanish, while the surviving even ones reflect the spin texture defined by $\mathbf{b}(\mathbf{k})$. That is, spin-charge conversion by (tunnel) injection through S is anisotropic, and the anisotropy is dictated by the shape of $\mathbf{b}(\mathbf{k})$. Note that if magnetic correlations penetrate into the SO region they will modify $\mathbf{b}(\mathbf{k})$ and thus the anisotropy, as shown below. These arguments are general but qualitative, as the coefficients of the expansion are unknown. For more quantitative statements we turn to microscopic simulations.

Numerics: LAO|STO junction – We consider the 5-terminal configuration of a recent experiment [38], see Fig. 3 (a): the bottom 2DEG ($z = 0$) is in contact with the upper magnetic electrode ($z > L_z$) via an extended barrier ($0 < z \leq L_z$). Given the existing effective models for LAO|STO 2DEGs [32, 34, 35], we focus on the d_{xz} - d_{yz} hybrid band to highlight the anisotropic character of tunneling spin galvanic physics in a minimal 2-band model. The effective Hamiltonian includes a 4-fold symmetric cubic Rashba term [34] and reads

$$H = \left[\frac{p^2}{2m} + U(z) \right] + \alpha_3(z) (p_x^2 - p_y^2) (\sigma^x p_y - \sigma^y p_x) - \frac{\Delta_{xc}(z)}{2} \mathbf{n}(\theta, \phi) \cdot \boldsymbol{\sigma} - \frac{\hbar^2 \partial_z^2}{2m}. \quad (13)$$

Here $\alpha_3(z) = \alpha_3 \exp(-z/\xi_\alpha)$ is the Rashba coupling constant, decaying to zero away from the 2DEG. The *s-d* exchange term $\Delta_{xc}(z) = \Delta_{xc} \exp[-(L_z - z)/\xi_{xc}]$ is instead at full strength in the magnetic electrode and vanishes away from it. The tunnel barrier $U(z)$ is a rectangular barrier of height U_0 , shown in black in Fig. 3 (a). The 3-dimensional scattering region is built by discretizing the Hamiltonian (13) on a cubic lattice of size $L_x = L_y = 50$ sites and height $L_z = 6$ sites. The $z = 0$ layer –

the 2DEG – is connected to four 2-dimensional leads along x and y , all normal ($\Delta_{xc} = 0, \alpha_3 = 0$). Each lead is $W_L = 30$ sites wide and attached centrally to the 2DEG layer. The upper contact is the M electrode ($\Delta_{xc} \neq 0, \alpha_3 = 0$). In a real setup the 2DEG modes have a finite extension along z , which allows coupling through the barrier and into M . To mimic the extension we model the extended barrier defined above as 3 transition layers just above the 2DEG, topped with two layers with on-site energy $U(z) = U_0 > \mu$ representing the tunnel barrier. With lattice spacing $a = 1$, we set the isotropic hopping parameter $t = 1$, and fix $\mu = 1.1, \alpha_3 = -0.2, \Delta_{xc} = -0.6, U_0 = 1.9, \xi_\alpha = 2L_z$. For $z = 0$ the on-site energy is $4t$, ensuring good coupling to the 2-dimensional leads, while it is $6t$ in the upper layers. We use the KWANT package [48] to compute the transmissions $T_{\alpha\beta}^{\sigma\sigma'}$ at energy μ . Details about the discretized model are found in the Appendix. The lead indices α, β are shown in Fig. 3, with B, F respectively labelling the B (ack) and F (ront) contacts. The resulting spin-charge conductance \mathcal{G}_{sc}^x along the x -axis,

$$\begin{aligned} \mathcal{G}_{sc}^x = \frac{1}{\mathcal{G}_M} & \left[\mathcal{G}_{LM} \left(\mathcal{G}_{RM}^\uparrow - \mathcal{G}_{RM}^\downarrow \right) - \mathcal{G}_{RM} \left(\mathcal{G}_{LM}^\uparrow - \mathcal{G}_{LM}^\downarrow \right) \right. \\ & + \left(\mathcal{G}_{LM}^\downarrow - \mathcal{G}_{RM}^\downarrow \right) \left(\mathcal{G}_{BM}^\uparrow + \mathcal{G}_{FM}^\uparrow \right) \\ & \left. - \left(\mathcal{G}_{LM}^\uparrow - \mathcal{G}_{RM}^\uparrow \right) \left(\mathcal{G}_{BM}^\downarrow + \mathcal{G}_{FM}^\downarrow \right) \right], \quad (14) \end{aligned}$$

is calculated at zero temperature and yields the current $I_{sc}^x = I_L - I_R = \mathcal{G}_{sc}^x \delta\mu_s / e$. The y -current $I_{sc}^y = I_B - I_F = \mathcal{G}_{sc}^y \delta\mu_s / e$ follows by exchanging $L \leftrightarrow B, R \leftrightarrow F$ in Eq.(14). Results for $\xi_{xc} = L_z$, which ensures that magnetic correlations are absent from the 2DEG, are shown in Figs. 3 (b), (c). The same data is shown as a 2D polar plot in (b) and as a 1D plot in (c). The overall spin-charge conversion (green curves) shows the 4-fold symmetry of the Rashba bands, as observed in experiments [38]. Detaching the y -leads to get the 3-terminal setup from Fig. 1 disentangles \mathcal{G}_{sc}^y (red triangles) from \mathcal{G}_{sc}^x . As expected, the two contributions differ only by a $\pi/2$ -shift. The response is however distorted if magnetic exchange below the tunnel barrier grows in strength, as shown in Figs. 3 (d), (e), where $\xi_{xc} = 2L_z$. The enhanced competition between SO and magnetism causes a splitting of the spin-charge conversion maxima, reflecting the distorted Fermi contours shown in the insets of panel (d).

Onsager reciprocity and anisotropies – The above clarifies why in the very same oxide 2DEG the ISGE is isotropic [40], while the SGE measured in a spin pumping setup is not: Onsager reciprocal quantities are not the current-induced spin polarisation on the 2DEG side, $\delta\mathbf{S}_{2DEG}$, and the spin polarisation-induced current on the same side, I_{2DEG} . They are rather the current I_{2DEG} and the non-equilibrium spin polarisation $\delta\mathbf{S}_M$ on the magnetic electrode side[49], *i.e.* the whole experimen-

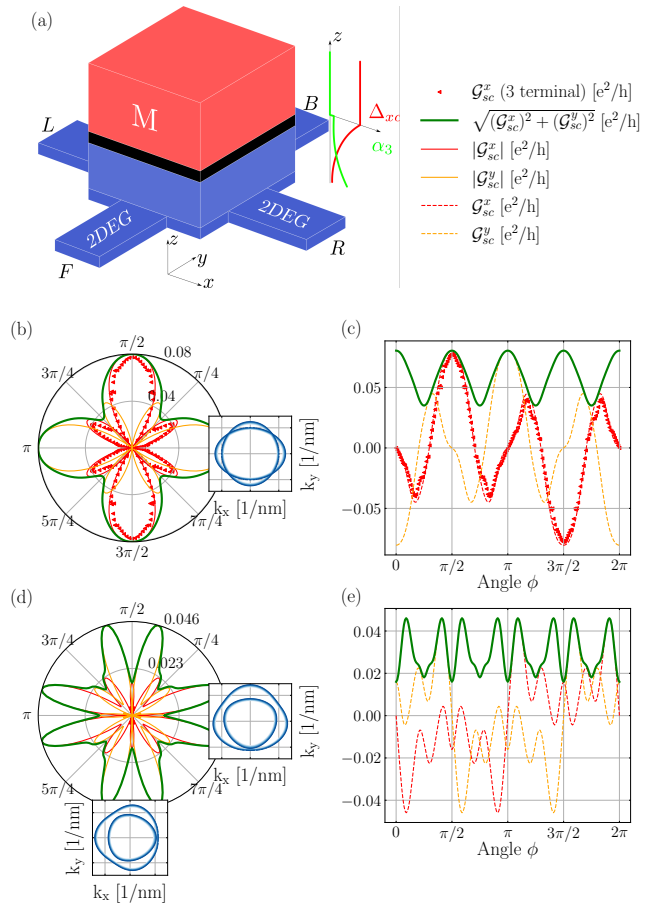


FIG. 3. (a) Schematic plot of 5 terminal setup. (b) to (e) numerical results of spin-charge conversion conductance for different values of ξ_{xc} . Parameters are specified in the main text. Insets: Fermi contour for $\alpha_3 = -0.2$ and $\Delta_{xc} = 0$ in (a) and $\Delta_{xc} = -0.6$ in (d) at $\phi = 0$ and $\phi = 3\pi/2$.

tal setup should be considered when discussing spin-charge reciprocity[50, 51]. The Landauer-Büttiker approach does this by default [52].

Conclusions – We identified and microscopically characterised the tunnelling anisotropic SGE taking place at an inversion symmetry-broken magnetic tunnel junction under a pure spin bias, as well as its reciprocal effect. Our theory is general and should thus be relevant in any multi-terminal junction where magnetization and spin-orbit coupling coexist. When applied to the specific case of an oxide-based spin pumping setup it provides a microscopic description of recent measurements and validates general phenomenological arguments [38]. We expect our framework and conclusions to apply to orbital angular momentum-to-charge conversion as well, which can be tackled following *e.g.* Ref. [53]. However a precise test for LAO|STO first requires a fully established low-energy model (see Ref. [54] for a recent attempt at building one).

Acknowledgements – CG thanks Michel Viret and

Alexander Smogunov for helpful discussions, and the STherQO members for useful comments. MB acknowledges support by the Deutsche Forschungsgemeinschaft (DFG, German Research Foundation) within Project-ID 314695032 – SFB 1277 (project A07).

Appendix: Tight-binding model

The five-terminal system sketched in Fig. 3(a) of the main text is modeled as follows. Space is discretized on a cubic grid with lattice spacing $a = 1$. Each site \mathbf{r}_i of coordinates $(x_i = ia, y_j = ja, z_k = ka)$ is labeled alternatively by the triplet (i, j, k) . The cubic scattering region S is made of a 2DEG portion of length L_x and width L_y lying in the plane $z = 0$, topped with $L_z - 1$ layers. Its tight-binding Hamiltonian reads

$$H_S = \sum_{\mathbf{r} \in S} c_{\mathbf{r}}^\dagger \left[\epsilon_0(z) + U(z) - \frac{\Delta_{xc}(z)}{2} \mathbf{n}(\theta, \phi) \cdot \boldsymbol{\sigma} \right] c_{\mathbf{r}} - t \sum_{\langle \mathbf{r}, \mathbf{r}' \rangle} c_{\mathbf{r}'}^\dagger c_{\mathbf{r}} + H_{SOC} \quad (15)$$

where t is the nearest neighbor hopping term, $\epsilon_0(z = 0) = 4t$ while $\epsilon_0(z \neq 0) = 6t$, $U(z) = U_0$ in the two top layers representing the tunnel barrier and 0 elsewhere, and $\Delta_{xc}(z) = \Delta_{xc} \exp[-(L_z - z)/\xi_{xc}]$ is the exchange term. The cubic Rashba SO coupling is accounted for by

$$H_{SOC} = -i \sum_{i,j,k} \frac{\alpha_3(z_i)}{8} \left[c_{i+3,j,k}^\dagger \sigma_y + c_{i,j+3,k}^\dagger \sigma_x - 4 c_{i+1,j+1,k}^\dagger (\sigma_x + \sigma_y) + 4 c_{i+1,j-1,k}^\dagger (\sigma_x - \sigma_y) + 5 c_{i+1,j,k}^\dagger \sigma_y + 5 c_{i,j+1,k}^\dagger \sigma_x \right] c_{i,j,k} + h.c. \quad (16)$$

obtained by discretizing the second term in the right-hand side of Eq. (13) of the main text and we take $\alpha_3(z) = \alpha_3 \exp(-z/\xi_\alpha)$. In the equations above, $c_{\mathbf{r}} \equiv c_{i,j,k} \equiv (c_{\mathbf{r}}^\uparrow, c_{\mathbf{r}}^\downarrow)$, $c_{\mathbf{r}}^\sigma$ being the annihilation operator of an electron at site \mathbf{r} with spin σ with respect to the z direction. The sum $\sum_{\langle \mathbf{r}, \mathbf{r}' \rangle}$ is restricted to nearest neighbors. The scattering region S is then attached with nearest neighbor hopping term t to four left (L), right (R), back (B), and front (F) leads of width W_L in the plane $z = 0$ (through the 2DEG) and to a fifth ferromagnetic lead M along $z > 0$ (through the barrier) as shown in Fig. 3(a). Their tight-binding Hamiltonians read

$$H_\alpha = -t \sum_{\langle \mathbf{r}, \mathbf{r}' \rangle} c_{\mathbf{r}'}^\dagger c_{\mathbf{r}} + 4t \sum_{\mathbf{r} \in \alpha} c_{\mathbf{r}}^\dagger c_{\mathbf{r}} \quad (17)$$

for $\alpha = L, R, B, F$, and

$$H_M = -t \sum_{\langle \mathbf{r}, \mathbf{r}' \rangle} c_{\mathbf{r}'}^\dagger c_{\mathbf{r}} + \sum_{\mathbf{r} \in M} c_{\mathbf{r}}^\dagger \left[6t - \frac{\Delta_{xc}}{2} \mathbf{n}(\theta, \phi) \cdot \boldsymbol{\sigma} \right] c_{\mathbf{r}} \quad (18)$$

for the ferromagnetic lead. Note that there is no cubic SOC in the leads and the exchange term amplitude is constant in M .

* cosimo.gorini@cea.fr

- [1] I. Žutić, J. Fabian, and S. Das Sarma, Spintronics: Fundamentals and applications, Rev. Mod. Phys. **76**, 323 (2004).
- [2] A. Fert and F. N. V. Dau, Spintronics, from giant magnetoresistance to magnetic skyrmions and topological insulators, C. R. Physique **20**, 817 (2019).
- [3] S. D. Ganichev, E. L. Ivchenko, V. V. Bel'kov, S. A. Tarasenko, M. Sollinger, D. Weiss, W. Wegscheider, and W. Prettl, Spin-galvanic effect, Nature **417**, 153 (2002).
- [4] S. D. Ganichev, P. Schneider, V. V. Bel'kov, E. L. Ivchenko, S. A. Tarasenko, W. Wegscheider, D. Weiss, D. Schuh, B. N. Murdin, P. J. Phillips, C. R. Pidgeon, D. G. Clarke, M. Merrick, P. Murzyn, E. V. Beringulin, and W. Prettl, Spin-galvanic effect due to optical spin orientation in n-type GaAs quantum well structures, Phys. Rev. B **68**, 081302(R) (2003).
- [5] E. L. Ivchenko and S. D. Ganichev, Spin-dependent photogalvanic effects (a review), arXiv, 1710.09223 (2017).
- [6] C. Gorini, A. M. Sheikhabadi, K. Shen, I. V. Tokatly, G. Vignale, and R. Raimondi, Theory of current-induced spin polarization in an electron gas, Phys. Rev. B **95**, 205424 (2017).
- [7] A. Maleki Sheikhabadi, I. Miatka, E. Y. Sherman, and R. Raimondi, Theory of the inverse spin galvanic effect in quantum wells, Phys. Rev. B **97**, 235412 (2018).
- [8] M. I. Dyakonov, Spin hall effect, in Spin Physics in Semiconductors (Springer, 2006) p. 211.
- [9] A. A. Bakun, B. P. Zakharchenya, A. A. Rogachev, M. N. Tkachuk, and V. G. Fleisher, Observation of a surface photocurrent caused by optical orientation of electrons in a semiconductor, JETP Lett. **40**, 1293 (1984).
- [10] S. O. Valenzuela and M. Tinkham, Direct electronic measurement of the spin hall effect, Nature **442**, 176 (2006).
- [11] C. Hahn, G. de Loubens, O. Klein, M. Viret, V. V. Naleto, and J. Ben Youssef, Comparative measurements of inverse spin hall effects and magnetoresistance in yig/pt and yig/ta, Phys. Rev. B **87**, 174417 (2013).
- [12] L. Liu, O. J. Lee, T. J. Gudmundsen, D. C. Ralph, and R. A. Buhrman, Current-induced switching of perpendicularly magnetized magnetic layers using spin torque from the spin hall effect, Phys. Rev. Lett. **109**, 096602 (2012).
- [13] M. Obstbaum, M. Härtinger, H. G. Bauer, T. Meier, F. Swientek, C. H. Back, and G. Woltersdorf, Inverse spin hall effect in ni₈₁fe₁₉/normal-metal bilayers, Phys. Rev. B **89**, 060407(R) (2014).
- [14] G. V. Karnad, C. Gorini, K. Lee, T. Schulz, R. L. Conte, A. W. J. Wells, D.-S. Han, K. Shahbazi, J.-S. Kim, T. A. Moore, H. J. M. Swagten, U. Eckern, R. Raimondi, and M. Kläui, Evidence for phonon skew scattering in the spin hall effect of platinum, Phys. Rev. B **97**, 100405 (2018).
- [15] J. C. R. Sánchez, L. Vila, G. Desfonds, S. Gambarelli, J. P. Attané, J. M. D. Teresa, C. Magén, and A. Fert, Spin-to-charge conversion using Rashba coupling at the interface between non-magnetic materials, Nat. Com-

- mun. **4**, 2944 (2013).
- [16] Y. Shiomi, K. Nomura, Y. Kajiwara, K. Eto, M. Nohak, K. Segawa, Y. Ando, and E. Saitoh, Spin-electricity conversion induced by spin injection into topological insulators, *Phys. Rev. Lett.* **113**, 196601 (2014).
- [17] J.-C. Rojas-Sánchez, S. Oyarzún, Y. Fu, A. Marty, C. Vergnaud, S. Gambarelli, L. Vila, M. Jamet, Y. Ohtsubo, A. Taleb-Ibrahimi, P. Le Fèvre, F. Bertran, N. Reyren, J.-M. George, and A. Fert, Spin to charge conversion at room temperature by spin pumping into a new type of topological insulator: α -sn films, *Phys. Rev. Lett.* **116**, 096602 (2016).
- [18] D. Bercioux and P. Lucignano, Quantum transport in rashba spin-orbit materials: a review, *Reports on Progress in Physics* **78**, 106001 (2015).
- [19] V. P. Amin and M. D. Stiles, Spin transport at interfaces with spin-orbit coupling: Formalism, *Phys. Rev. B* **94**, 104419 (2016).
- [20] F. Hellman, A. Hoffmann, Y. Tserkovnyak, G. S. D. Beach, E. E. Fullerton, C. Leighton, A. H. MacDonald, D. C. Ralph, D. A. Arena, H. A. Dürr, P. Fischer, J. Grollier, J. P. Heremans, T. Jungwirth, A. V. Kimel, B. Koopmans, I. N. Krivorotov, S. J. May, A. K. Petford-Long, J. M. Rondinelli, N. Samarth, I. K. Schuller, A. N. Slavin, M. D. Stiles, O. Tchernyshyov, A. Thiaville, and B. L. Zink, Interface-induced phenomena in magnetism, *Rev. Mod. Phys.* **89**, 025006 (2017).
- [21] Z. Wen, Z. Qiu, S. Tölle, C. Gorini, T. Seki, D. Hou, T. Kubota, U. Eckern, E. Saitoh, and K. Takahashi, Spin-charge conversion in mnmbs heusler alloy films, *Sci. Adv.* **5**, eaaw9337 (2019).
- [22] V. T. Pham, H. Yang, W. Y. Choi, A. Marty, I. Groen, A. Chuvilin, F. S. Bergeret, L. E. Hueso, I. V. Tokatly, and F. Casanova, Large spin-charge interconversion induced by interfacial spin-orbit coupling in a highly conducting all-metallic system, *Phys. Rev. B* **104**, 184410 (2021).
- [23] J. Fabian, A. Matos-Abiague, C. Ertler, P. Stano, and I. Žutić, Semiconductor spintronics, *Act. Phys. Slov.* **57**, 565 (2007).
- [24] A. Matos-Abiague and J. Fabian, Anisotropic tunneling magnetoresistance and tunneling anisotropic magnetoresistance: Spin-orbit coupling in magnetic tunnel junctions, *Phys. Rev. B* **79**, 155303 (2009).
- [25] A. Matos-Abiague and J. Fabian, Tunneling anomalous and spin hall effects, *Phys. Rev. Lett.* **115**, 056602 (2015).
- [26] Under-the-barrier spin-charge effects are fundamental in strongly disordered systems, see Ref. [55].
- [27] T. H. Dang, H. Jaffrès, T. L. Hoai Nguyen, and H.-J. Drouhin, Giant forward-scattering asymmetry and anomalous tunnel hall effect at spin-orbit-split and exchange-split interfaces, *Phys. Rev. B* **92**, 060403 (2015).
- [28] I. V. Rozhansky, D. Q. To, H. Jaffrès, and H.-J. Drouhin, Chirality-induced tunneling asymmetry at a semiconductor interface, *Phys. Rev. B* **102**, 045428 (2020).
- [29] D. Q. To, T. H. Dang, L. Vila, J. P. Attané, M. Bibes, and H. Jaffrès, Spin to charge conversion at rashba-split srTiO_3 interfaces from resonant tunneling, *Phys. Rev. Research* **3**, 043170 (2021).
- [30] A. Ohtomo and H. Hwang, A high-mobility electron gas at the $\text{LaAlO}_3/\text{SrTiO}_3$ heterointerface, *Nature* **427**, 423 (2004).
- [31] N. Reyren, S. Thiel, A. D. Caviglia, L. F. Kourkoutis, G. Hammerl, C. Richter, C. W. Schneider, T. Kopp, A.-S. Rüetschi, D. Jaccard, M. Gabay, D. A. Müller, J.-M. Triscone, and J. Mannhart, Superconducting interfaces between insulating oxides, *Science* **317**, 1196 (2007).
- [32] D. C. Vaz, P. Noël, A. Johansson, B. Göbel, F. Y. Bruno, G. Singh, S. McKeown-Walker, F. Trier, L. M. Vicente-Arche, A. Sander, S. Valencia, P. Bruneel, M. Vivek, M. Gabay, N. Bergeal, F. Baumberger, H. Okuno, A. Barthélémy, A. Fert, L. Vila, I. Mertig, J.-P. Attané, and M. Bibes, Mapping spin-charge conversion to the band structure in a topological oxide two-dimensional electron gas, *Nat. Mater.* **18**, 1187 (2019).
- [33] P. Noël, F. Trier, L. M. V. Arche, J. Bréhin, D. C. Vaz, V. Garcia, S. Fusil, A. Barthélémy, L. Vila, M. Bibes, and J.-P. Attané, *Nature* **580**, 483 (2020).
- [34] J. Zhou, W.-Y. Shan, and D. Xiao, Spin responses and effective hamiltonian for the two-dimensional electron gas at the oxide interface $\text{LaAlO}_3/\text{SrTiO}_3$, *Phys. Rev. B* **91**, 241302(R) (2015).
- [35] G. Seibold, S. Caprara, M. Grilli, and R. Raimondi, Theory of the spin galvanic effect at oxide interfaces, *Phys. Rev. Lett.* **119**, 256801 (2017).
- [36] E. Bousquet, M. Dawber, N. Stucki, C. Lichtensteiger, P. Hermet, S. Gariglio, J.-M. Triscone, and P. Ghosez, Improper ferroelectricity in perovskite oxide artificial superlattices, *Nature* **452**, 732 (2008).
- [37] S. Valencia, A. Crassous, L. Bocher, V. Garcia, X. Moya, R. O. Cherifi, C. Deranlot, K. Bouzehouane, S. Fusil, A. Zolli, A. Gloter, N. D. Mathur, A. Gaupp, R. Abrudan, F. Radu, A. Barthélémy, and M. Bibes, Interface-induced room-temperature multiferroicity in BaTiO_3 , *Nat. Mater.* **10**, 753 (2011).
- [38] A. E. Hamdi, J.-Y. Chauleau, M. Boselli, C. Thibault, C. Gorini, A. Smogunov, C. Barreateau, S. Gariglio, J. M. Triscone, and M. Viret, Observation of the inverse orbital rashba-edelstein effect, Under evaluation (2022).
- [39] Ref. [38] also discusses orbital angular momentum-to-charge conversion. Here we focus on spin-charge conversion and only comment on orbital physics in the closing.
- [40] A. Johansson, B. Göbel, J. Henk, M. Bibes, and I. Mertig, Spin and orbital edelstein effects in a two-dimensional electron gas: Theory and application to SrTiO_3 interfaces, *Phys. Rev. Research* **3**, 013275 (2021).
- [41] O. Rousseau, C. Gorini, F. Ibrahim, J.-Y. Chauleau, A. Solognac, A. Hallal, S. Tölle, M. Chshiev, and M. Viret, Spin-charge conversion in ferromagnetic rashba states, *Phys. Rev. B* **104**, 134438 (2021).
- [42] S. Tölle, U. Eckern, and C. Gorini, Spin-charge coupled dynamics driven by a time-dependent magnetization, *Phys. Rev. B* **95**, 115404 (2017).
- [43] A. Kara Slimane, P. Reck, and G. Fleury, Simulating time-dependent thermoelectric transport in quantum systems, *Phys. Rev. B* **101**, 235413 (2020).
- [44] See Ref. [56] for a similar discussion in a related context.
- [45] We choose the energy reference so that $\mu_L = \mu_0 - \delta\mu_{LR}/2$, $\mu_R = \mu_0 + \delta\mu_{LR}/2$.
- [46] F. Zhai and H. Q. Xu, Symmetry of spin transport in two-terminal waveguides with a spin-orbital interaction and magnetic field modulations, *Phys. Rev. Lett.* **94**, 246601 (2005).
- [47] P. Jacquod, R. Whitney, J. Meair, and M. Büttiker, Onsager relations in coupled electric, thermoelectric and spin transport: The ten-fold way, *Phys. Rev. B* **86**,

- 155118 (2012).
- [48] C. W. Groth, M. Wimmer, A. R. Akhmerov, and X. Waintal, Kwant: a software package for quantum transport, *New J. Phys.* **16**, 063065 (2014).
- [49] The polarizations are integrals over the 2DEG surface/M electrode volume of the respective surface/volume densities $\delta s_{2\text{DEG}}$, δs_M .
- [50] L. Y. Wang, A. G. Mal'shukov, and C. S. Chu, Nonuniversality of the intrinsic inverse spin-hall effect in diffusive systems, *Phys. Rev. B* **85**, 165201 (2012).
- [51] C. Gorini, R. Raimondi, and P. Schwab, Onsager relations in a two-dimensional electron gas with spin-orbit coupling, *Phys. Rev. Lett.* **109**, 246604 (2012).
- [52] Reciprocity in the presence of SO is delicate but can be properly handled with other approaches, see *e.g.* [6, 51, 55, 57, 58] and references therein. For more examples of Landauer-Büttiker calculations see [59, 60].
- [53] J. Shi, G. Vignale, D. Xiao, and Q. Niu, Quantum theory of orbital magnetization and its generalization to interacting systems, *Phys. Rev. Lett.* **99**, 197202 (2007).
- [54] M. Trama, V. Cataudella, C. A. Perroni, F. Romeo, and R. Citro, Gate tunable anomalous hall effect: Berry curvature probe at oxides interfaces, *Phys. Rev. B* **106**, 075430 (2022).
- [55] D. S. Smirnov and L. E. Golub, Electrical spin orientation, spin-galvanic, and spin-hall effects in disordered two-dimensional systems, *Phys. Rev. Lett.* **118**, 116801 (2017).
- [56] R. Rouzegar, L. Brandt, L. Nadvornik, D. A. Reiss, A. L. Chekhov, O. Gueckstock, C. In, M. Wolf, T. Seifert, P. W. Brouwer, G. Woltersdorf, and T. Kampfrath, Laser-induced terahertz spin transport in magnetic nanostructures arises from the same force as ultrafast demagnetization, *Phys. Rev. B* **106**, 144427 (2022).
- [57] N. Sugimoto, S. Onoda, S. Murakami, and N. Nagaosa, Spin hall effect of a conserved current: Conditions for a nonzero spin hall current, *Phys. Rev. B* **73**, 113305 (2006).
- [58] K. Shen, R. Raimondi, and G. Vignale, Microscopic theory of the inverse edelstein effect, *Phys. Rev. Lett.* **112**, 096601 (2014).
- [59] I. Adagideli, M. Scheid, M. Wimmer, G. E. W. Bauer, and K. Richter, Extracting current-induced spins: spin boundary conditions at narrow hall contacts, *New J. Phys.* **9**, 382 (2007).
- [60] I. Adagideli, V. Lutsker, M. Scheid, P. Jacquod, and K. Richter, Spin transistor action from hidden onsager reciprocity, *Phys. Rev. Lett.* **108**, 236601 (2012).